Hindawi
Wireless Communications and Mobile Computing
Volume 2022, Article ID 4089931, 13 pages
https://doi.org/10.1155/2022/4089931

Research Article

Time-Division Multiarray Beamforming for UAV Communication

Zhengxiang Duan, Xin Yang, Qian Xu, and Ling Wang

School of Electronics and Information, Northwestern Polytechnical University, Xi'an 710072, China

Correspondence should be addressed to Xin Yang; xinyang@nwpu.edu.cn

Received 20 October 2021; Revised 23 February 2022; Accepted 24 March 2022; Published 12 April 2022

Academic Editor: Guangwei Yang

Recently, unmanned aerial vehicles (UAVs) have been widely used in various industries. However, the communication links of UAVs are also threatened by eavesdropping. To enhance physical layer security (PLS) for UAV communications, a time-division multiarray beamforming (TDMB) scheme is proposed. Multiple antenna arrays steer their beamforming vectors based on their position relative to the legitimate user (LU). Thus, angle-distance-dependent directional modulation (DM) can be achieved. Time-division means multiple antenna arrays take turns transmitting different symbols from a same packet. The receiver in undesired directions suffers from intersymbol interference (ISI) because of the path differences between the receiver and different antenna arrays. This paper shows the signal-to-interference-plus-noise ratio (SINR) distribution with the proposed method in a 2-dimensional plane. Also, the improvement of the secrecy rate with the proposed method under different total antennas and artificial noise power is studied. Overall, these results indicate that the security rate has improved more with the proposed method, where the numbers of antennas and the power of AN are limited. Therefore, this method is suitable for UAV security communication.

1. Introduction

The number of unmanned aerial vehicles (UAVs) has experienced explosive growth in the past decade, whether for agriculture, industrial, or civilian use. Wireless communication is a key technique for UAVs. It is used for wireless control and broadcasting data from the sensor network. Nevertheless, information disclosure is inevitable due to the openness of wireless channels. This might lead to property loss. In severe cases, people can be injured. A widely adopted approach to alleviating this problem is encryption. However, it may not be straightforward to use in UAV communications due to the complexity of key distribution and management. In recent decades, physical layer security (PLS) has aroused great research interest among researchers [1]. The basic idea of PLS is to utilize the randomness of the wireless channel to realize secure communication [2]. Since the PLS technique is primarily a signal processing technology, it can be used in conjunction with encryption.

Directional modulation (DM) is one of the most important PLS techniques. It can transmit digital modulated signals to intended spatial directions while twisting the constellations of these signals in all other directions [3]. A method named dual-beam DM was introduced in [4]. In this technique, I and Q data are transmitted by different antennas. However, the synchronization of the I and Q data from different antennas is not taken into consideration. An antenna subset modulation scheme was introduced in [5], where different antenna subsets transmit different symbols from a same packet. However, this method only achieves angle-dependent DM. Artificial noise (AN) can also be employed in DM for a further improvement of the security. The use of AN is to reduce the signal-to-interference-to-noise ratio (SINR) in undesired directions. The AN was used in DM for the first time in [6]. Taking into account the imperfect channel state information (CSI), robust AN-based methods for single-beam and multibeam DM were proposed in [7, 8], respectively. The projection matrix of AN can be

constructed by zero-forcing [9], null-space projection [10], or iteration convex optimization methods [11]. Directional modulation for different types of arrays is also a research hotspot, including the switched antenna array [12], the intelligent reflecting surfaces (IRS) [13], the 4-D antenna array [14, 15], the frequency diverse array (FDA) [16, 17], and the multiple antenna arrays (MAAs) [18]. A spread-spectrum directional modulation technique based on a switched antenna array is proposed in [12]. With the spread-spectrum technique, a low probability of detection is achieved. In [13], a new secure transmission scheme aided by the IRS is proposed. This method can reduce costs and save energy. Another cost-saving method is proposed in [14, 15], which replaces the phase shifter with high-speed RF switches. At the same time, the accuracy of phase shift becomes higher. An FDA scheme is proposed to achieve angle-distance-dependent DM in [16, 17]. In [18], the author also realized angle-distance-dependent DM by MAAs. However, the signals from different arrays will interfere with each other at the receiver, when MAAs transmit in the same frequency band simultaneously. A recent study in [21] proposed a PLS algorithm for UAV communication using linear virtual antenna array (VAA). The random location perturbations of the VAA elements were used to randomize radiation patterns at eavesdroppers (Eves).

In conclusion, despite the various advantages of the aforementioned DM schemes, some problems need to be overcome.

(1) The methods proposed in [4–15] only work when Eves and legitimate users (LUs) are not in the same direction. In other words, when Eves and LUs lie on the same line, the transmission will be unsafe

(2) Most of the above-mentioned methods are complex in the calculation. To improve security performance, the number of antennas and the power of AN need to be increased. It is not suitable for UAV scenarios

Aiming at addressing these problems, we propose a time-division multiarray beamforming (TDMB) scheme to achieve secure and precise transmission. Multiple antenna arrays steer their beamforming vectors based on their position relative to the LU. Time-division means multiple antenna arrays take turns transmitting different symbols from a same packet. The path differences between the receiver and different antenna arrays will cause intersymbol interference (ISI) at the receiver. However, with the knowledge of the LU's precise location, the ISI at LU can be completely removed. Therefore, the received signals of Eves will not only suffer from constellation distortion but also be affected by ISI. In this way, we narrow the unsafe area from "lines" to "points." The main contributions of this paper can be summarized as follows:

(1) We propose a time-division multiarray beamforming scheme, which realizes angle-distance-dependent DM

(2) We improve security performance through ISI rather than increasing the number of antennas or the power of AN

(3) The proposed method has low computational complexity. And it has better security performance with a small number of antennas or low power of AN

Hereafter, the paper is organized as follows. In Section 2, an MAA model is introduced. Section 3 proposes a TDMB scheme. Section 4 analyses the secrecy rate and the symbol error rate (SER). The secrecy performance is evaluated by several numerical results in Section 5. Finally, Section 6 concludes the paper. Tables 1 and 2 summarize the abbreviations and notations of symbols in this paper.

2. System Model

The application scenario of the proposed method is shown in Figure 1. There are three types of UAV, namely, the transmitter, the LU, and Eves. The transmitter sends information through multiple antenna arrays to the LU. Meanwhile, the transmitter transmits AN to interfere with Eves. Eves could be anywhere in the space and try to intercept the information from the transmitter.

We consider the case where a transmitter is equipped with N ($N \geq 2$) non-collocated antenna arrays, of which the spacing is L. Each antenna array is an M-element isotropic uniform linear array (ULA) with spacing $d = \lambda/2 (L \gg d)$. λ is the wavelength of the carrier. The MAA system model in the XOY plane is presented in Figure 2. All antennas are on the x-axis. The first antenna of the first array is at the origin of the coordinate axis. Without loss of generality, the first antenna element of each ULA is selected as the reference antenna for that ULA. The coordinates of the receiver are (x, y). r_n and θ_n are the distance and direction angle between the nth transmit antenna array and the receiver, respectively. For the far-field model, it is reasonable to adopt the approximation $r_n \approx r_n - (m-1)d \sin \theta_n$. As depicted in Figure 2, we can obtain the geometric relationship

$$r_n = \sqrt{[x - (n-1)L]^2 + y^2}, \tag{1}$$

$$\theta_n = \arctan\left((x - (n-1)L)/y\right). \tag{2}$$

The far-field beam pattern of the MAA model with beamforming factor $w_{n,m}$ in the location (x, y) can be expressed as

$$F(r_1, \theta_1, \cdots, r_N, \theta_N) = e^{j2\pi f_c t} \sum_{n=1}^{N} \sqrt{\rho_n} e^{-j2\pi f_c (r_n/c)} \sum_{m=1}^{M} w_{n,m} e^{2\pi f_c (m-1) d \sin \theta_n / c}, \tag{3}$$

where c is the speed of light, f_c is the carrier frequency, t is the propagation time, $w_{n,m}$ is the beamforming factor for the mth ($m = 1, 2, \cdots, M$) antenna at the nth ($n = 1, 2, \cdots, N$) transmit antenna array. ρ_n refers to the path loss factor from the nth array to the receiver. The path loss factor

Table 1: Abbreviations in the paper.

Abbreviation	Meaning	Abbreviation	Meaning
AA	Antenna array	AN	Artificial noise
AWGN	Additive white Gaussian noise	BER	Bit error rate
CSI	Channel state information	DM	Directional modulation
Eve	Eavesdropper	FDA	Frequency diverse array
FPGA	Field programmable gate array	IRS	Intelligent reflecting surfaces
ISI	Intersymbol interference	LOS	Line-of-sight
LU	Legitimate user	MAA	Multiple antenna array
PLS	Physical layer security	QPSK	Quadrature phase-shift keying
SER	Symbol error rate	SINR	Interference-plus-noise ratio
SNR	Signal-to-noise ratio	TDMB	Time-division multiarray beamforming
UAV	Unmanned aerial vehicle	ULA	Uniform linear array
VAA	Linear virtual antenna array		

Table 2: Notations of symbols in the paper.

Symbol	Meaning	Symbol	Meaning
$\mathbb{N}^+$	Positive integer field	$\mathbb{C}$	Complex number field
$(\cdot)^T$	Transpose	$(\cdot)^H$	Hermitian transport
N	Number of antenna arrays	L	Spacing of antenna arrays
M	Number of antennas in an array	d	Spacing of array elements
λ	Wavelength of the carrier	c	Speed of light
f_c	Carrier frequency	P_s	Power for transmitting symbols
P_A	Power for AN	a_i	Normalized QPSK constellation mapping
T	Symbol duration	Q	Total number of symbols in a packet
σ_l^2	The noise variance received by LU	$\mathbf{h}_{l,n}$	Steering vector from LU to the nth antenna array
$\mathbf{h}_{e,n}$	Steering vector from the nth antenna array to Eve	$\sigma_{e,n}^2$	Noise variance received by Eve
R_l	Achievable rates of LU	$\overline{\gamma_e}$	Average SINR of Eve
R_s	Secrecy rate	R_e	Achievable rates of Eve
P_{se}	Symbol error rate	P_b	Bit error rate

decreases slowly when the distance is far enough. Then, we can approximate that $\rho_1 \approx \rho_n$. For simplicity, we define $\rho \triangleq \rho_n$. Equation (3) can be written as

$$F(r_1, \theta_1, \cdots, r_N, \theta_N) \triangleq e^{j2\pi f_c t}\sqrt{\rho}\sum_{n=1}^{N} e^{-j2\pi f_c(r_n/c)}\sum_{m=1}^{M} w_{n,m}e^{2\pi f_c(m-1)d\ \sin\theta_n/c}. \tag{4}$$

The normalized steering vector of the nth transmit antenna array in position (r_n, θ_n) can be expressed as

$$\mathbf{h}_n(r_n, \theta_n) = \sqrt{\frac{\rho}{M}}\left[e^{j\Phi_n(1)}, e^{j\Phi_n(2)}, \cdots, e^{j\Phi_n(M)}\right]^T, \tag{5}$$

where $\Phi_n(m)$ is given by

$$\Phi_n(m) = \frac{2\pi f_c(m-1)d\ \sin\theta_n}{c}. \tag{6}$$

To simplify the expression, we define $\mathbf{h}_n \triangleq \mathbf{h}_n(r_n, \theta_n)$. The far-field beam pattern of the MAA model is actually a superposition of radiation from multiple arrays, i.e.,

$$F(r_1, \theta_1, \cdots, r_N, \theta_N) \triangleq \sum_{n=1}^{N} \mathbf{h}_n^H \mathbf{w}_n e^{-j2\pi f_c(t-(r_n/c))}, \tag{7}$$

where $\mathbf{w}_n = [w_{n,1}, w_{n,2}, \cdots, w_{n,M}]^T \in \mathbb{C}^{M\times 1}$ is the transmit beamforming vector.

3. The Proposed TDMB Scheme

In this section, we propose a TDMB scheme, where different antenna arrays take turns to transmit different symbols of a same packet, as illustrated in Figure 3. In this way, the message transmitted by each array is incomplete. Only in the intersection area of different beams can complete information be obtained, while other places suffer from severe ISI.

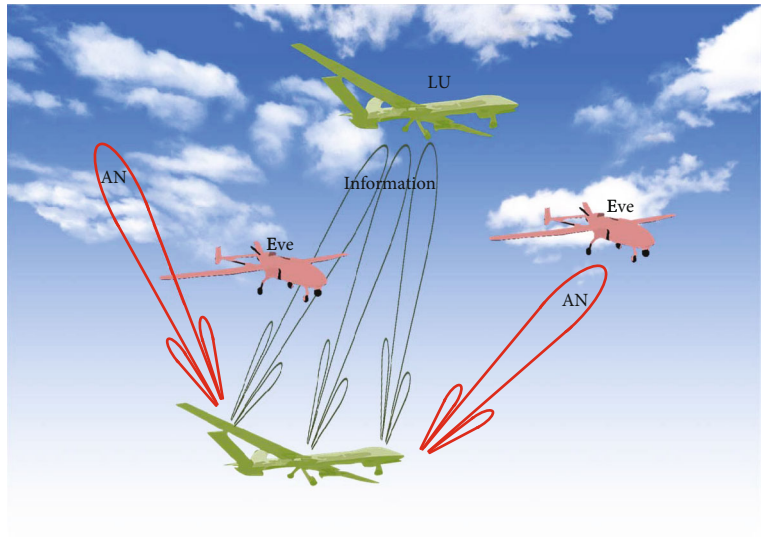

Figure 1: The application scenario of the proposed method. There are three types of UAVs, namely, the transmitter, the legitimate user, and eavesdroppers.

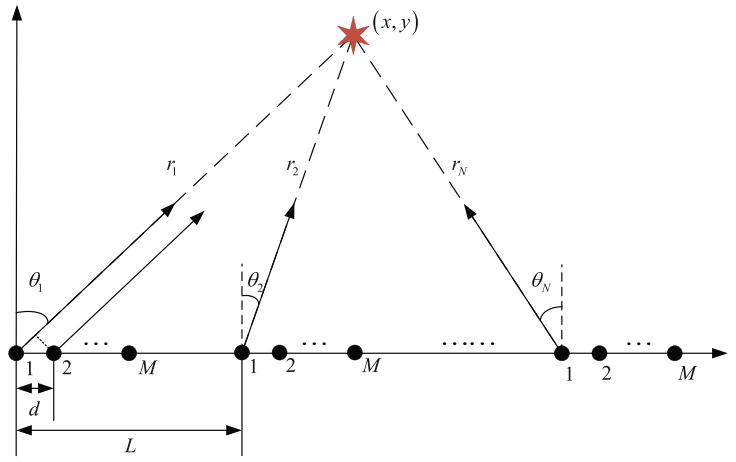

Figure 2: System model of MAA.

3.1. Transmitted Signal Model. As shown in Figure 3, the baseband signal of the nth antenna array is given by

$$\mathbf{s}_n(t) = \sqrt{P_s}\mathbf{w}_n x_n(t-(n-1)T+\tau_{l,n})e^{j2\pi f_c \tau_{l,n}} + \sqrt{P_A}\mathbf{n}_{A,n}(t), \tag{8}$$

where P_s and P_A are the power for transmitting symbols and AN, respectively. T is the symbol duration, and $\mathbf{n}_{A,n}(t)$ is the normalized M-tuple AN waveform, which is given by

$$\mathbf{n}_{A,n}(t) = \mathbf{T}_n \mathbf{z}_n(t), \tag{9}$$

where $\mathbf{z}_n(t) \in \mathbb{C}^{M\times 1}$ is a waveform following $\mathcal{CN}(\mathbf{0}_{M\times 1}, \mathbf{I}_M)$ distribution, $\mathbf{T}_n \in \mathbb{C}^{M\times M}$ refers to the projection matrix of AN. Since $\mathbf{z}_n(t)$ obeys a Gaussian distribution at any moment, it can be regarded as a time-independent additive noise. We are more concerned with the statistical properties of $\mathbf{z}_n(t)$ and $\mathbf{n}_{A,n}(t)$ such as variance rather than the exact value at a given moment. Therefore, the subsequent part of the paper abbreviates $\mathbf{z}_n(t)$ and $\mathbf{n}_{A,n}(t)$ as $\mathbf{z}_n$ and $\mathbf{n}_{A,n}$, respectively. Define (x_l, y_l) as the coordinate of LU, which can be transferred to angle $\theta_{l,n}$ and distance $r_{l,n}$ relative to the nth antenna array. The time difference between the signals transmitted from the nth array and from the first array to LU is denoted as $\tau_{l,n} = (r_{l,n} - r_{l,1})/c$. $x_n(t)$ in (8) represents the quadrature phase-shift keying (QPSK) modulated symbol of the nth array at time instant t, given by

$$x_n(t) = \sum_{k=0}^{Q/N-1} a_{kN+n} g(t-kNT), \tag{10}$$

where k represents the indexes of symbols transmitted by the nth antenna array, e.g., the first antenna array transmits $\{a_1, a_{N+1}, a_{2N+1}, \cdots, a_{kN+1}\}$with $a_i \in 1/\sqrt{2}\{1+j, 1-j, -1+j, -1-j\}$, $\forall i \in \mathbb{N}^+$, representing the normalized QPSK constellation mapping, Q is the total number of symbols in a

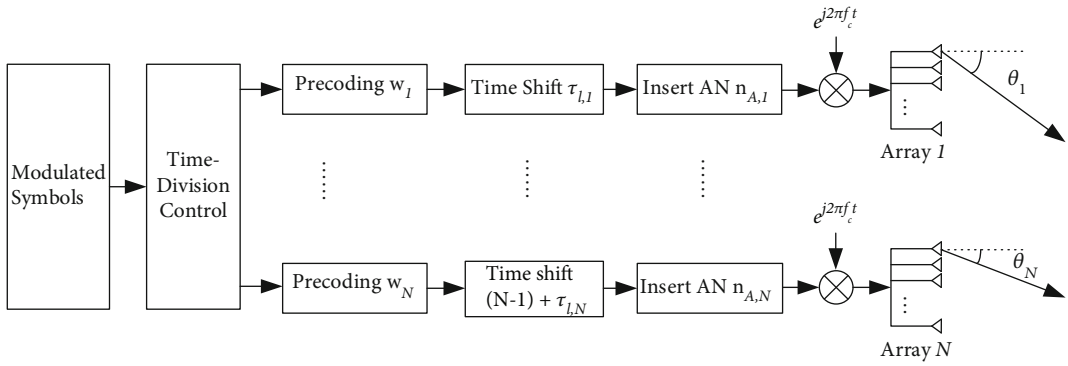

Figure 3: The architecture of the transmitter for the proposed TDMB scheme.

packet. Q is divisible by N. The ideal sinc pulse $g(t)$ is expressed as

$$g(t) = \frac{T}{\pi t} \sin\left(\frac{\pi t}{T}\right). \tag{11}$$

From (10), we can obtain the relationship between the transmitted symbols of each array and the total symbols. This describes how to do time division in the proposed TDMB scheme.

Next, we discuss how to design the transmit beamforming vector $\mathbf{w}_n$ and the projection matrix of AN $\mathbf{T}_n$. After being transmitted through a wireless line-of-sight (LOS) channel, LU will receive mixed signals from different arrays. For notational simplicity, we use $\mathbf{h}_{l,n} \in \mathbb{C}^{M\times 1}$ to denote the steering vector from LU to the nth antenna array, i.e., $\mathbf{h}_{l,n} \triangleq \mathbf{h}_n(r_{l,n}, \theta_{l,n})$. Since the positions of Eves are unknown, to maximize the signal-to-noise ratio (SNR) at LU, the transmit beamforming vector $\mathbf{w}_n$ is designed as

$$\mathbf{w}_n = \frac{\mathbf{h}_{l,n}}{\sqrt{\rho}}. \tag{12}$$

For a further improvement of transmission security, AN is employed. To prevent the LU from being interfered by AN, we project the AN into the null space of the steering vector $\mathbf{h}_{l,n}$. Therefore, the projection matrix of AN $\mathbf{T}_n$ is given by

$$\mathbf{T}_n = \mathbf{I}_M - \frac{1}{\rho}\mathbf{h}_{l,n}\mathbf{h}_{l,n}^H. \tag{13}$$

According to (5), the projection matrix $\mathbf{T}_n$ and the steering vector $\mathbf{h}_{l,n}$ are orthogonal, as shown by

$$\begin{aligned}\mathbf{h}_{l,n}^H\mathbf{T}_n &= \mathbf{h}_{l,n}^H\left(\mathbf{I}_M - \frac{1}{\rho}\mathbf{h}_{l,n}\mathbf{h}_{l,n}^H\right)\\ &= \mathbf{h}_{l,n}^H - \frac{1}{\rho}\mathbf{h}_{l,n}^H\mathbf{h}_{l,n}\mathbf{h}_{l,n}^H\\ &= \mathbf{0}.\end{aligned} \tag{14}$$

3.2. Received Signal Model. According to (7) and (8), the signal received at LU can be given by

$$\begin{aligned}y_l(t) &= \sum_{n=1}^{N}\mathbf{h}_{l,n}^H\mathbf{s}_n\left(t - \frac{r_{l,n}}{c}\right)e^{j2\pi f_c(t-(r_{l,n}/c))} + n_l\\ &= e^{j2\pi f_c(t-(r_{l,1}/c))}\sum_{n=1}^{N}\mathbf{h}_{l,n}^H\mathbf{s}_n\left(t - \frac{r_{l,1}}{c} - \tau_{l,n}\right)e^{-j2\pi f_c\tau_{l,n}} + n_l,\end{aligned} \tag{15}$$

where n_l is the additive white Gaussian noise (AWGN) at LU with $n_l \sim \mathcal{CN}(0, \sigma_l^2)$ and σ_l^2 denotes the noise variance received by LU. Supposing the carrier exp $(j2\pi f_c(t - r_{l,1}/c))$ is perfectly removed and timing synchronization is well done, the received baseband signal is given by

$$r_l(t) = \sum_{n=1}^{N}\mathbf{h}_{l,n}^H\mathbf{s}_n(t - \tau_{l,n})e^{-j2\pi f_c\tau_{l,n}} + n_l. \tag{16}$$

Substituting (8), (10), and (14) into (16), $r_l(t)$ can be simplified as

$$\begin{aligned}r_l(t) &= \sum_{n=1}^{N}\mathbf{h}_{l,n}^H\left[\sqrt{P_s}\mathbf{w}_n x_n(t-(n-1)T)e^{j2\pi f_c\tau_{l,n}} + \sqrt{P_A}\mathbf{n}_{A,n}\right]e^{-j2\pi f_c\tau_{l,n}} + n_l\\ &\triangleq \sqrt{\rho P_s}\sum_{k'=0}^{Q-1}a_{k'+1}g\left(t - k'T\right) + n_l,\end{aligned} \tag{17}$$

where k' is the index of symbols in a packet. A detailed derivation of the (17) is provided in Appendix. Since the path delay from the antenna arrays to LU is considered at the transmitter, the received symbol interval is equal to symbol duration time T, which means there is no ISI at the LU.

Similarly, the received signal at Eve is given by

$$y_e(t) = \sum_{n=1}^{N} \mathbf{h}_{e,n}^H \mathbf{s}_n \left(t - \frac{r_{e,n}}{c}\right) e^{j2\pi f_c (t-(r_{e,n}/c))} + n_e$$
$$= e^{j2\pi f_c (t-(r_{e,1}/c))} \sum_{n=1}^{N} \mathbf{h}_{e,n}^H \mathbf{s}_n \left(t - \frac{r_{e,1}}{c} - \tau_{e,n}\right) e^{-j2\pi f_c \tau_{e,n}} + n_e, \tag{18}$$

where n_e is the AWGN at Eve with $n_e \sim \mathcal{CN}(0, \sigma_e^2)$ and $\sigma_{e,n}^2$ denotes the noise variance received by Eve; $r_{e,n}$ and $\mathbf{h}_{e,n} \in \mathbb{C}^{M\times 1}$, respectively, refer to the distance and steering vector from the nth antenna array to Eve. The time difference between the signals transmitted from the nth array and from the first array to Eve is denoted as $\tau_{e,n} = (r_{e,n} - r_{e,1})/c$. Under this circumstance, the carrier and delay time are $\exp(j2\pi f_c (t - r_{e,1}/c))$ and $r_{e,1}/c$, respectively. Thus, the baseband signal of Eve is given by

$$r_e(t) = \sum_{n=1}^{N} \mathbf{h}_{e,n}^H \left[\sqrt{P_s}\mathbf{w}_n x_n (t-(n-1)T + \tau_{l,n} - \tau_{e,n}) e^{j2\pi f_c \tau_{l,n}} + \sqrt{P_A}\mathbf{n}_{A,n}\right] e^{-j2\pi f_c \tau_{e,n}} + n_e$$
$$= \sqrt{P_s} \sum_{n=1}^{N} \mathbf{h}_{e,n}^H \mathbf{w}_n x_n (t-(n-1)T - \Delta\tau_n) e^{-j2\pi f_c \Delta\tau_n} + \sqrt{P_A} \sum_{n=1}^{N} \mathbf{h}_{e,n}^H \mathbf{n}_{A,n} e^{-j2\pi f_c \tau_{e,n}} + n_e \tag{19}$$
$$= \underbrace{\sqrt{P_s}\sum_{n=1}^{N}\sum_{k=0}^{Q/N-1} \mathbf{h}_{e,n}^H \mathbf{w}_n a_{kN+n} g(t-(kN+n-1)T - \Delta\tau_n) e^{-j2\pi f_c \Delta\tau_n}}_{\text{ISI}} + \underbrace{\sqrt{P_A}\sum_{n=1}^{N} \mathbf{h}_{e,n}^H \mathbf{n}_{A,n} e^{-j2\pi f_c \tau_{e,n}}}_{\text{AN}} + n_e,$$

where $\Delta\tau_n = \tau_{e,n} - \tau_{l,n}$ represents the time differences between the propagation time from the antenna arrays to the Eve and LU. Indeed, the ISI at Eve is caused by $\Delta\tau_n$.

It can be observed from (17) and (19) that symbols received by Eve are disturbed by three factors:

(1) Amplitude and phase of received signals vary because of multiarray DM. $\mathbf{h}_{e,n}^H \mathbf{w}_n$ indicates that the constellation diagram of the received signal in the nondesired direction will be distorted. $\sum_{n=1}^{N} \mathbf{h}_{e,n}^H \mathbf{w}_n$ represents that only in the intersection area of different beams can signals be correctly obtained. These results show that the MAA model can realize angle-distance-dependent DM

(2) Received signals suffer from ISI because of time division. $g(t-(kN+n-1)T - \Delta\tau_n)$ indicates that the interval between adjacent sinc pulses is not equal to T when $\Delta\tau_n \neq 0$. This will cause ISI, as shown in Figure 4. Meanwhile, $\Delta\tau_n$ is determined by the position of receivers

(3) AN. Similar to multiarray DM, only the receiver at the desired location is free from AN

4. Performance Analysis

In this section, the secrecy rate and SER for the proposed beamforming scheme are analysed. To facilitate analysis, we assume that all AWGNs are normalized and have the same distribution with zero mean and variance σ^2 for both LUs and Eves.

4.1. Secrecy Rate. According to (17), the SINR of LU can be expressed as

$$\gamma_l = \frac{\rho P_s}{\sigma^2}. \tag{20}$$

In light of (19), the interference of Eve consists of AN and ISI. The power of received AN can be expressed as

$$P_{r,A} = P_A \sum_{n=1}^{N} \left|\mathbf{h}_{e,n}^H \mathbf{T}_n\right|^2. \tag{21}$$

Assume that Eves know the positions of LU and antenna arrays, which means Eves can sample at the best time by calculating the path difference, i.e., sample time-
$t \in \{(kN+n-1)T + \Delta\tau_n, k = 0, 1, \cdots, Q/N-1, n = 1, \cdots, N\}$. Since the transmit period can be regarded as NT, we only need to analyse the aliasing of N symbols, i.e., the 2nd symbol to the $(N+1)$th symbol. For simplicity, we only consider the interference from the immediately preceding and following symbols, since that from the rest symbols is negligible. Then, the power of ISI for the lth symbol can be expressed as

$$P_{l,\text{ISI}} = P_s \left[\left|g(T + \Delta\tau_l - \Delta\tau_{l-1})\mathbf{h}_{e,l-1}^H \mathbf{w}_{l-1}\right|^2 + \left|g(T + \Delta\tau_{l+1} - \Delta\tau_l)\mathbf{h}_{e,l+1}^H \mathbf{w}_{l+1}\right|^2\right],$$
$$l = 2, \cdots, N+1, \tag{22}$$

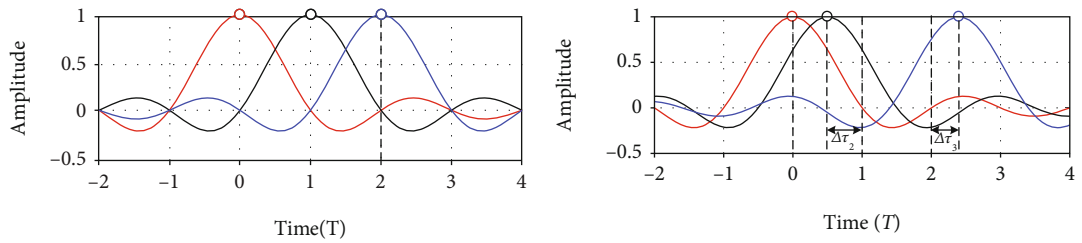

FIGURE 4: The three received symbols of (a) LU and (b) Eve. In (a), each symbol is not disturbed by other symbols. In (b), each symbol suffers from ISI which is determined by $\Delta\tau_n$.

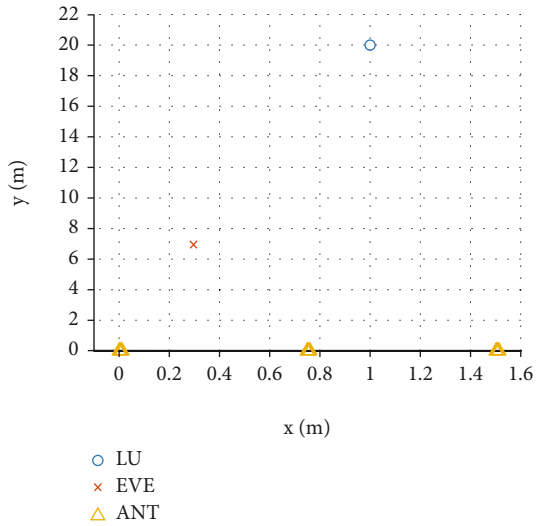

FIGURE 5: The position of LU, Eve, and antenna arrays in a 2-dimensional plane.

where $\Delta\tau_{N+1} = \Delta\tau_1$, $\Delta\tau_{N+2} = \Delta\tau_2$, $\mathbf{w}_{N+1} = \mathbf{w}_1$, $\mathbf{w}_{N+2} = \mathbf{w}_2$, $\mathbf{h}_{e,N+1} = \mathbf{h}_{e,1}$, and $\mathbf{h}_{e,N+2} = \mathbf{h}_{e,2}$, because of cyclicity. Considering that the ISI is different for each symbol, we calculate the average SINR of Eve, which is given by

$$\overline{\gamma_e} = \frac{1}{N^2}\sum_{l=2}^{N+1}\frac{P_s\sum_{n=1}^{N}\left|\mathbf{h}_{e,n}^H\mathbf{w}_n\right|^2}{\left(P_{l,\mathrm{ISI}} + P_{r,A} + \sigma^2\right)}. \tag{23}$$

According to (20) and (23), the achievable rates of LU and Eve can be calculated, respectively, by

$$R_l = \log_2(1+\gamma_l), \tag{24}$$

$$R_e = \log_2(1+\overline{\gamma_e}). \tag{25}$$

Then, the secrecy rate can be defined as

$$R_s \triangleq \max\{R_l - R_e, 0\}. \tag{26}$$

4.2. SER. To evaluate the communication performance, we are interested in bit error rate (BER) and SER. The BER with the best detection and perfect recovery for QPSK is given by [19]

$$P_b = Q\left(\sqrt{2\gamma_b}\right), \tag{27}$$

where $Q(z) = 1/\sqrt{2\pi}\int_z^\infty \exp(-z^2/2)dz$ is the tail distribution function of the standard normal distribution and $\gamma_b = E_b/N_0$ represents the SNR per bit. The relationship between γ_b and the SNR per symbol γ_s for M-PSK modulation leads to the approximations

$$\gamma_b \approx \frac{\gamma_s}{\log_2 M}. \tag{28}$$

Substituting (28) into (27), we get P_b for QPSK as

$$P_b = Q(\sqrt{\gamma_s}). \tag{29}$$

In systems with interference, we use SINR instead of SNR to calculate the BER. Then, we can obtain P_b for LU and Eve, respectively, as

$$P_{b,l} = Q(\sqrt{\gamma_l}), \tag{30}$$

$$P_{b,e} = Q\left(\sqrt{\overline{\gamma_e}}\right). \tag{31}$$

The SER is equal to the error probability of any bit in a symbol, which is given by

$$P_{se} = 1 - (1-P_b)^2. \tag{32}$$

5. Simulation Results

In this section, the proposed TDMB scheme is evaluated in terms of SINR distribution, secrecy rate, and SER. The carrier frequency is set as $f_c = 30$ GHz. Consider a scenario with limited resources, i.e., UAV, which means large-scale antenna arrays are not permitted. Assume that there is $N = 3$ transmit antenna arrays with $M = 4$ elements for each ULA. The spacing of the array elements and antenna arrays are $d = c/2f_c$ and $L = 150d$, respectively. Thus, the coordinates of arrays are (0 m, 0 m), (0.75 m, 0 m), and (1.5 m, 0 m). The coordinates of LU and Eve are (1 m, 20 m) and (0.3 m, 7 m), respectively, as shown in Figure 5. The baseband modulation is QPSK with symbol rate $R_s = 2$ Gsps, which satisfies the narrow-band assumption. The required SNR for the received signals at LU is 15 dB, which remains unchanged in the simulations. We assume that the noise

Table 3: Simulation parameters.

Parameters	Value
Number of antenna arrays, N	3
Number of ULA elements, M	4
Carrier frequency, f_s	30 GHz
Spacing of array elements, d	0.5 cm
Spacing of antenna arrays, L	0.75 m
Coordinates of arrays	(0 m, 0 m), (0.75 m, 0 m), and (1.5 m, 0 m)
Coordinate of LU	(1 m, 20 m)
Coordinate of Eve	(0.3 m, 7 m)
Modulation mod	QPSK
Symbol rate, R_s	2 Gsps
Power for transmitting symbols, P_s	3.07 dBm
Power for AN, P_A	0.06 dBm
Noise power	-100 dBm

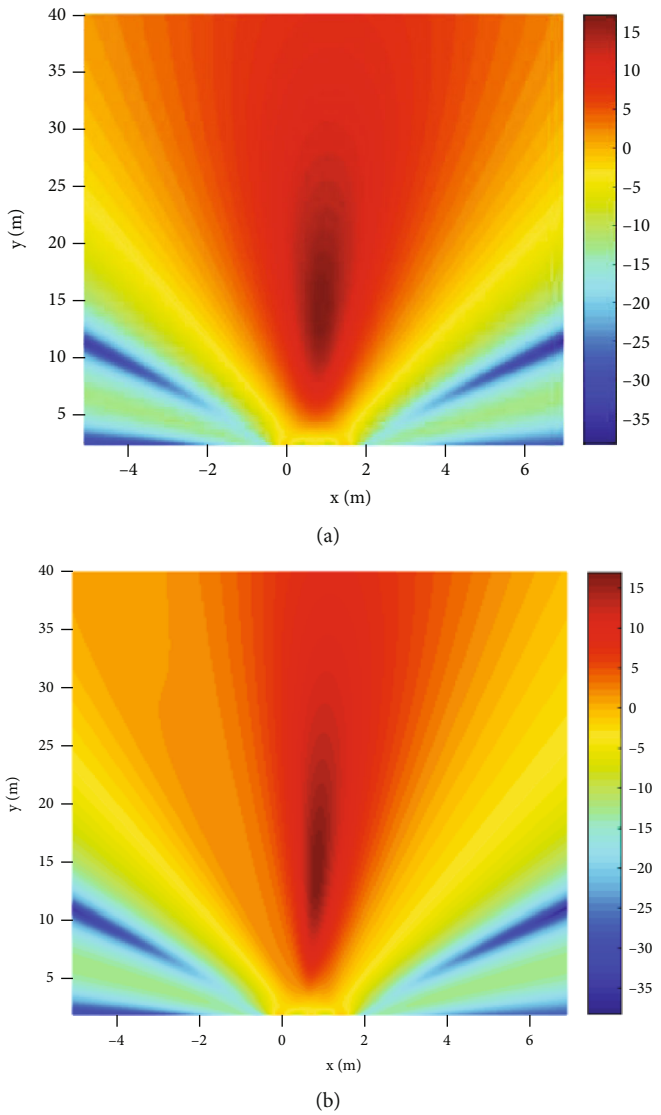

Figure 6: The SINR (dB) distribution in a 2-dimensional plane (a) method in [18] and (b) proposed TDMB scheme.

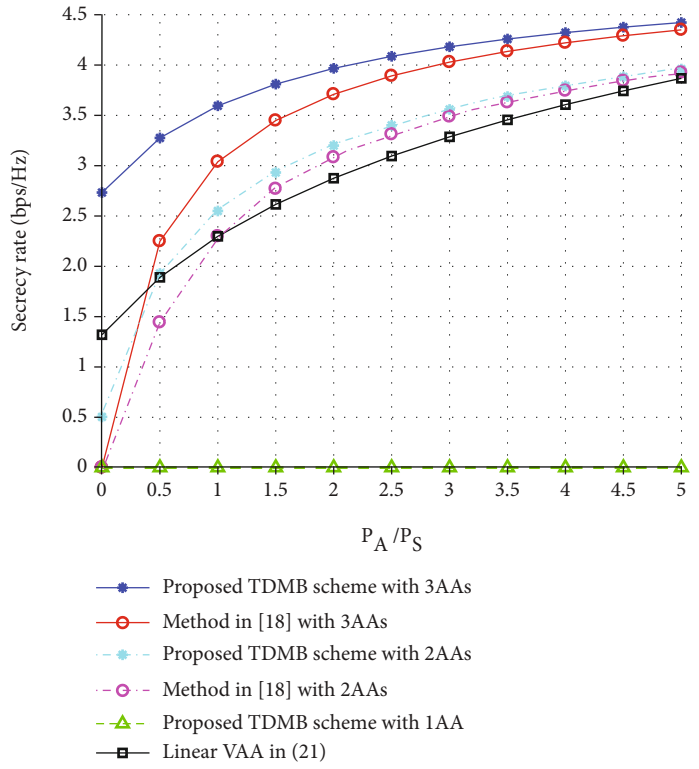

FIGURE 7: The secrecy rate (bps/Hz) versus the power of AN normalized by transmission power for different numbers of antenna arrays and methods, where the total number of antennas MN = 12 (applies also to VAA). Transmit power of VAA is $(P_A + P_s)$.

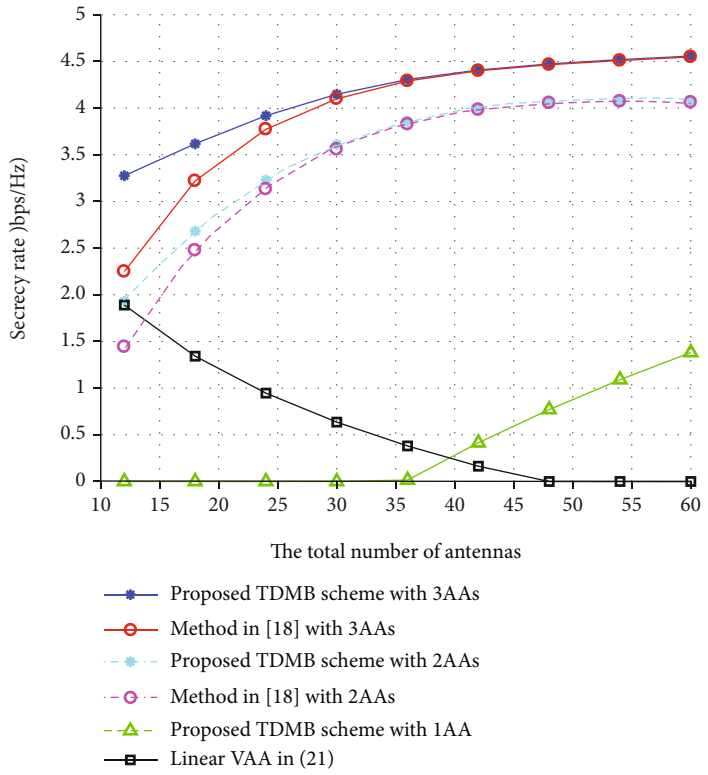

FIGURE 8: The secrecy rate (bps/Hz) versus the total number of antennas for different numbers of antenna arrays and methods, where $P_A/P_s = 1/2$. Transmit power of VAA is $(P_A + P_s)$.

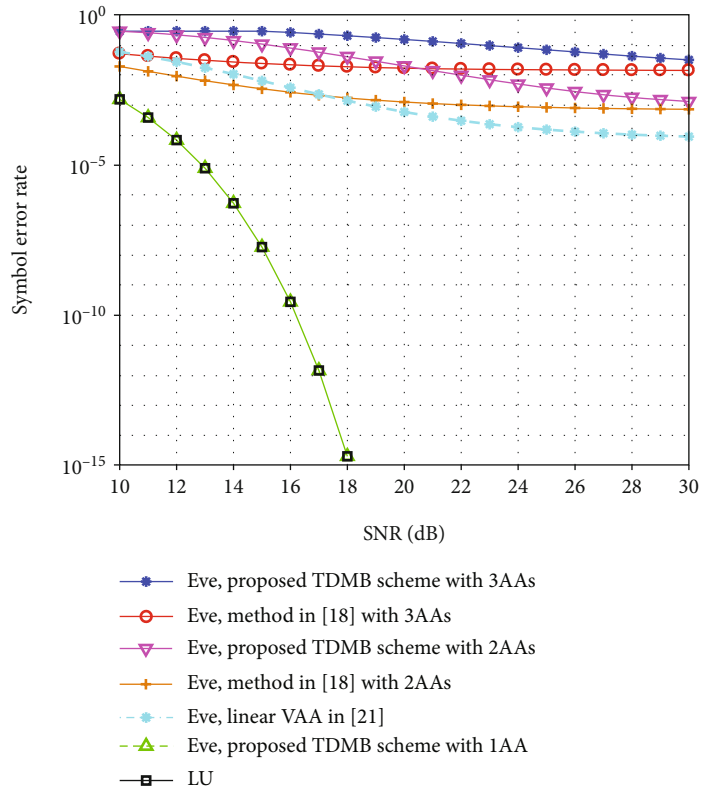

Figure 9: The SER versus SNR for different numbers of antenna arrays and methods, where $P_A/P_s = 1/2$.

power is -100 dBm. By means of the radio wave propagation loss in the free space [20], the path loss factor ρ is given by

$$\mathrm{Lfs(dB)} = 32.5 + 20\ \mathrm{lg}\ [f_c(\mathrm{MHz})] + 20\ \mathrm{lg}\ [r(\mathrm{Km})]. \quad (33)$$

Based on the location of LU, it can be calculated that P_s needs to be 3.07 dBm. Considering that there is not much power for AN, the power of AN is set to be $P_A = 1/2P_s$. Unless otherwise stated, the default simulation parameters are summarized in Table 3.

In Figure 6, we compare the SINR of the proposed scheme with the method in [18]. The signal models in Figure 6 are both three antenna arrays (AAs). Figure 6(b) shows the SINR of the proposed TDMB scheme which exploits the ISI, while Figure 6(a) shows the SINR of the method in [18]. Deeper red indicates higher SINR. As expected, the SINR at LU is 15 dB, which meets our requirement. It can be seen from Figure 6 that the deepest red area is an ellipse rather than a line. This shows that the MAA scheme performs well against eavesdroppers close to the transmitter. In other words, it proves that angle-distance-dependent DM is achieved with MAA. Comparing Figures 6(a) and 6(b), it can be observed that with the help of time-division scheme, the SINR for the region far from LU decreases more significantly; e.g., the area with SINR greater than 10 decreased from 55 m^2 to 29 m^2, which indicates that the proposed scheme can further improve the secrecy performance.

In Figure 7, we investigate the secrecy rate versus the power of AN for different numbers of antenna arrays and methods. We compared the TDMB scheme with the method in [18, 21]. The total number of antennas is set as MN = 12 (applies also to VAA). The position of Eve is chosen as (0.3,7), which has a similar direction angle as LU. The secrecy rate of the method in [21] increases monotonically with increasing distribution length L. So, we set the L of VAA to be 1.5 m in agreement with the 3AAs. Since the method in [21] does not use AN, we assume that the total transmit power is consistent with the TDMB scheme; i.e., the transmit power of VAA is $(P_A + P_s)$. The following simulation of the method in [21] is the same. When the number of antenna arrays is 1, the TDMB scheme is degraded to normal single-beam DM. As shown in Figure 7, the secrecy rate for one antenna array is zero. This indicates that a single array cannot achieve secrecy transmission when the Eves and LU are in the same direction. Conversely, when the number of arrays is greater than one, partial secrecy transmission can be achieved even if Eves and LU are in the same direction of a given array. In addition, it can be observed that the ISI caused by the time-division scheme can significantly improve the secrecy rate when AN is unused. Meanwhile, the interference caused by the random location perturbations of the VAA elements is between the ISI of 3AAs and 2AAs. When P_A/P_s is greater than 0.5, the secrecy rate of the TDMB scheme with 2AAs is greater than the method in [21]. With the increase of the power for AN, the secrecy rate tends to be constant. Because $\Delta\tau_n$ is a variable independent of the power of AN,

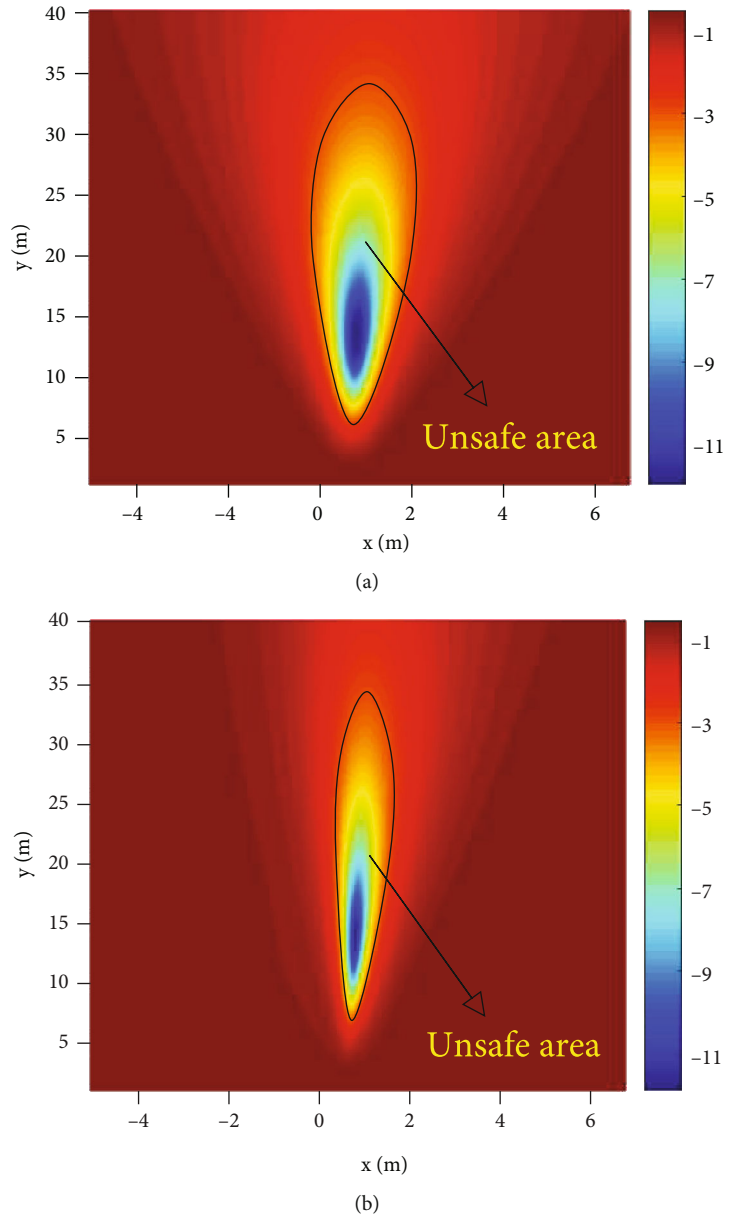

Figure 10: The logarithmic SER distribution in a 2-dimensional plane (a) method in [18] and (b) proposed TDMB scheme.

the ISI remains unchanged for the same position. Therefore, with increasing AN power, the impact of ISI on the secrecy rate gradually decreases. Moreover, the upper bound of the secrecy rate improves with the enhancement of the number of antenna arrays. Figure 7 proves that the time-division scheme contributes to the enhancement of the secrecy rate, especially when there is not enough power for AN.

In Figure 8, we investigate the secrecy rate versus the total number of antennas MN for different numbers of antenna arrays and methods. As shown in Figure 8, for a fixed small number of total antennas, the performance gap between the method in [18] and the TDMB scheme is larger for the case "3AAs" than "2AAs". When the total number of antennas is fixed and limited, the number of antennas per array decreases as the number of antenna arrays increases, which means that the beamwidth for each antenna array becomes wider. With a wider beamwidth, i.e., a larger numerator in (23), ISI plays a more important role in reducing Eve's SINR. When the total number of antennas is the same, the greater the number of arrays, the higher the upper bound of the secrecy capacity. Meanwhile, the greater the number of arrays, the greater the improvement from the time-division scheme. This is because when the number of arrays increases, the scale of MAA will become larger. This results in larger values of $\Delta\tau_n$ as well. With an increasing total number of antennas, the impact of ISI on the secrecy rate gradually decreases. Surprisingly, the secrecy rate using VAA in [21] decreases as the number of antennas increases. According to Equation (24) [21], when the total power is fixed, the SINR of the Eves increase as the number of antennas increases. When the number of antennas reaches

36, the beamwidth of the single antenna array is narrow enough to avoid the Eves. At this point, the secrecy rate starts to be greater than 0. Therefore, the proposed scheme is more suitable for the situation that the number of antennas is limited.

In Figure 9, we investigate the SER versus the SNR for different numbers of antenna arrays and methods. Since we assume the noise power is the same throughout the space, the SNR is determined by the transmit power P_s. The SER level reflects SINR. First, we note that since Eve and LU are basically in the same direction, Eve does not suffer from interference in the case with 1AA. The curve of Eve of the TDMB scheme with 1AA coincides with that of LU. According to Equations (21), (22), (23), and (24) [21], each factor of the numerator and denominator in the SINR formula contains P_s except for the noise power (simplified as $\mathrm{SINR} = aP_s/(bP_s + c)$). This indicates that as P_s increases, the impact of noise power reduces. Eventually, the SINR will converge to a constant a/b. When the number of antenna arrays is the same, the TDMB scheme has a higher SER than the method in [18]. Factor a of the two methods is the same, while factor b of the TDMB scheme is greater than that of the method in [18] because of the ISI caused by the time-division scheme. Similarly, the greater the number of arrays, the higher the SER. The SER of the method in [21] is first higher than 2AAs but eventually less than 2AAs. The reason is that the method in [21] has a greater factor c/b. When P_s is insufficient, factor c plays a more important role. However, the interference caused by random location perturbations of the VAA elements is less than AN and ISI; i.e., the method in [21] has a greater factor a/b. As a result, the method in [21] has a lower SER. Theoretically, the TDMB scheme with 3AAs should have a lower SINR than that with 2AAs, but their SER is the same when the SNR is 10. The reason is that the upper limit of SER, 0.75, is reached.

Figure 10 compares the SER performance surface of the proposed TDMB scheme and the method in [18]. Consistent with the SINR distribution in Figure 6, the regions near LU enjoy a low SER. Note that the effects of path differences on the SER performance are asymmetric, although the path differences are symmetric. The ISI caused by increasing the received symbol interval is less than the ISI caused by decreasing the symbol interval. For example, we can see from Figure 4 that the second symbol moves closer to the first one when $\Delta\tau_2 < 0$. Assuming a new case with $\Delta\tau_2{}' = -\Delta\tau_2$, the second symbol will be further away from the first. It is easy to find that the first symbol receives more interference in the first case. Suppose that when the SER is greater than 10^{-5}, the Eves cannot eavesdrop on the information normally. Then, we can define an unsafe area, where the SER is lower than 10^{-3}. When the Eves are in an unsafe area, confidential transmission is not possible. We can use some physical methods to ensure that there are no Eves in unsafe areas, such as establishing cordon areas. Finally, as illustrated in Figure 10, the proposed method can improve security performance by utilizing ISI in the undesired directions with only limited resources.

6. Conclusions

In this paper, we investigated the PLS problem for UAV communications using the TDMB scheme. In the TDMB scheme, multiple antenna arrays steer their beamforming vectors based on their position relative to the legitimate user (LU). Meanwhile, multiple antenna arrays take turns transmitting different symbols from a same packet. We studied both analytically and through simulation the secrecy rate and SER of the received signals at different positions. We also simulated the secrecy rate under different total antennas and artificial noise power. These results suggested that the proposed method can achieve angle-distance-dependent DM. Moreover, the path differences between the receiver and different antenna arrays can cause ISI for receivers in undesired directions. Hence, the security performance is further enhanced. These results also suggested that the security rate has a greater improvement with the proposed method, where the number of antennas and the power of AN are limited. Therefore, this method is suitable for UAV security communication. Many UAVs are now equipped with antenna arrays. Although there is a loss in performance, MAAs can be implemented using subarrays. This does not require changes to the structure of the existing UAV, only modifications to the programmable part of the hardware, such as the field programmable gate array (FPGA). Alternatively, clustered UAV systems can be used to achieve MAAs, which requires the cluster to complete the networking first. The proposed method also has some drawbacks. First, it is only effective for phase-shift keying modulated. Second, when resources are sufficient, this method does not improve security performance much.

Further research is needed to investigate the beamforming scheme based on a uniform planar array. It is closer to practical application. The research scene will change from a 2-dimensional plane to a 3-dimensional space. Additional analysis of highly dynamic UAVs or mobile communications is also required.

Appendix

Here, we show the mathematical derivation of (17). By substituting (10), (12), and (14) into (17), we can get

$$\begin{aligned} r_l(t) &= \sum_{n=1}^{N} \mathbf{h}_{l,n}^H \left[\sqrt{P_s}\mathbf{w}_n x_n(t-(n-1)T) e^{j2\pi f_c \tau_{l,n}} + \sqrt{P_A}\mathbf{n}_{A,n} \right] e^{-j2\pi f_c \tau_{l,n}} + n_l \\ &= \sqrt{P_s} \sum_{n=1}^{N} \mathbf{h}_{l,n}^H \mathbf{w}_n x_n(t-(n-1)T) + n_l = \sqrt{\rho P_s} \sum_{n=1}^{N} x_n(t-(n-1)T) + n_l \\ &= \sqrt{\rho P_s} \sum_{n=1}^{N} \sum_{k=0}^{Q/N-1} a_{kN+n} g(t-(kN+n-1)T) + n_l. \end{aligned} \tag{A.1}$$

We expand the double summation

$$\sum_{n=1}^{N} \sum_{k=0}^{Q/N-1} kN + n, \tag{A.2}$$

to obtain each addend

$$\begin{matrix} 0+1 & 0+2 & \cdots & 0+N \\ N+1 & N+2 & \cdots & 2N \\ \vdots & \vdots & \ddots & \vdots \\ Q-N+1 & Q-N+2 & \cdots & Q \end{matrix}. \tag{A.3}$$

It can be seen from (A.3) that (A.2) can be rewritten as

$$\sum_{n=1}^{N}\sum_{k=0}^{Q/N-1} kN+n \triangleq \sum_{k'=0}^{Q-1} k'+1. \tag{A.4}$$

Substituting (A.4) into (A.1), (17) can be obtained as

$$r_l(t) \triangleq \sqrt{\rho P_s}\sum_{k'=0}^{Q-1} a_{k'+1}\, g\left(t-k'T\right)+n_l, \tag{A.5}$$

which completes the derivation.

Data Availability

No data were used to support this study.

Conflicts of Interest

The authors declare no conflicts of interest.

Acknowledgments

This work was supported in part by the National Natural Science Foundation of China under Grant Nos. 61901390 and 61901382.

References

[1] A. Mukherjee, S. A. A. Fakoorian, J. Huang, and A. L. Swindlehurst, "Principles of physical layer security in multiuser wireless networks: a survey," *IEEE Communications Surveys Tutorials*, vol. 16, no. 3, pp. 1550–1573, 2014.

[2] G. Zheng, I. Krikidis, J. Li, A. P. Petropulu, and B. Ottersten, "Improving physical layer secrecy using full-duplex jamming receivers," *IEEE Transactions on Signal Processing*, vol. 61, no. 20, pp. 4962–4974, 2013.

[3] F. Shu, T. Shen, L. Xu et al., "Directional modulation: a physical-layer security solution to B5G and future wireless networks," *IEEE Network*, vol. 34, no. 2, pp. 210–216, 2020.

[4] T. Hong, M.-Z. Song, and Y. Liu, "Dual-beam directional modulation technique for physical-layer secure communication," *IEEE Antennas and Wireless Propagation Letters*, vol. 10, pp. 1417–1420, 2011.

[5] N. Valliappan, A. Lozano, and R. W. Heath, "Antenna subset modulation for secure millimeter-wave wireless communication," *IEEE Transactions on Communications*, vol. 61, no. 8, pp. 3231–3245, 2013.

[6] O. N. Alrabadi and G. F. Pedersen, "Directional space-time modulation: a novel approach for secured wireless communication," in *In 2012 IEEE International Conference on Communications (ICC)*, pp. 3554–3558, Ottawa, ON, Canada, 2012.

[7] J. Hu, F. Shu, and J. Li, "Robust synthesis method for secure directional modulation with imperfect direction angle," *IEEE Communications Letters*, vol. 20, no. 6, pp. 1084–1087, 2016.

[8] F. Shu, X. Wu, J. Li, R. Chen, and B. Vucetic, "Robust synthesis scheme for secure multi-beam directional modulation in broadcasting systems," *IEEE Access*, vol. 4, pp. 6614–6623, 2016.

[9] T. Xie, J. Zhu, and Y. Li, "Artificial-noise-aided zero-forcing synthesis approach for secure multi-beam directional modulation," *IEEE Communications Letters*, vol. 22, no. 2, pp. 276–279, 2018.

[10] F. Shu, L. Xu, J. Wang, W. Zhu, and Z. Xiaobo, "Artificial-noise-aided secure multicast precoding for directional modulation systems," *IEEE Transactions on Vehicular Technology*, vol. 67, no. 7, pp. 6658–6662, 2018.

[11] R. M. Christopher and D. K. Borah, "Iterative convex optimization of multi-beam directional modulation with artificial noise," *IEEE Communications Letters*, vol. 22, no. 8, pp. 1712–1715, 2018.

[12] T. Hong, M.-Z. Song, and Y. Liu, "RF directional modulation technique using a switched antenna array for communication and direction-finding applications," *Progress In Electromagnetics Research*, vol. 120, pp. 195–213, 2011.

[13] L. Lai, J. Hu, Y. Chen, H. Zheng, and N. Yang, "Directional modulation-enabled secure transmission with intelligent reflecting surface," in *In 2020 IEEE 3rd International Conference on Information Communication and Signal Processing (ICICSP)*, pp. 450–453, Shanghai, China, 2020.

[14] Q. Zeng, P. Yang, H. Lin, F. Yang, and S. Yang, "Generalized closed-form sidebands radiation expressions for 4-D antenna arrays," *IEEE Transactions on Antennas and Propagation*, vol. 69, no. 2, pp. 1193–1197, 2021.

[15] G. Huang, Y. Ding, and S. Ouyang, "Multicarrier directional modulation symbol synthesis using time-modulated phased arrays," *IEEE Antennas and Wireless Propagation Letters*, vol. 20, no. 4, pp. 567–571, 2021.

[16] B. Qiu, M. Tao, L. Wang, J. Xie, and Y. Wang, "Multi-beam directional modulation synthesis scheme based on frequency diverse array," *IEEE Transactions on Information Forensics and Security*, vol. 14, no. 10, pp. 2593–2606, 2019.

[17] J. Xie, B. Qiu, Q. Wang, and J. Qu, "Broadcasting directional modulation based on random frequency diverse array," *Wireless Communication and Mobile Computing*, vol. 2019, no. 1, pp. 1–11, 2019.

[18] W. Zhang, M. Le, B. Li, J. Wang, and J. Peng, "Directional modulation-enhanced multiple antenna arrays for secure and precise wireless transmission," *Sensors*, vol. 19, no. 22, p. 4833, 2019.

[19] Q. Cheng, V. Fusco, J. Zhu, S. Wang, and F. Wang, "WFRFT-aided power-efficient multi-beam directional modulation schemes based on frequency diverse array," *IEEE Transactions on Wireless Communications*, vol. 18, no. 11, pp. 5211–5226, 2019.

[20] A. Goldsmith, *Wireless Communication*, Cambridge Univ. Press, Cambridge, U.K., 2007.

[21] H. Jung, S.-W. Ko, and I.-H. Lee, "Secure transmission using linearly distributed virtual antenna array with element position perturbations," *IEEE Transactions on Vehicular Technology*, vol. 70, no. 1, pp. 474–489, 2021.